Miniaturized Via-Free Magneto-Electric Dipole Antenna Fed by Substrate Integrated Coaxial Line on Reactive Impedance Surface

Tsz Ming Wong, Kwai Man Luk, *Fellow*, *IEEE*, and Kin Fai Tong, *Fellow*, *IEEE*

Abstract—A wideband via-free magneto-electric (ME) dipole antenna is conceived for millimeter wave band applications. Herein, the electric dipole patch and a half-wavelength radiating slot are excited in phase on the patch layer by a substrate integrated coaxial line (SICL) to fulfill the complementary conditions as a ME dipole. The proposed antenna omits the deployment of the vertically oriented shorted patch, which relieves the typical quarter-wavelength height constraint and fabrication complexity of the conventional ME dipole antennas. The antenna is further loaded with the capacitive reactive impedance surface (RIS) to achieve size miniaturization and bandwidth enhancement. The finalized dimension (excluding the RIS) is $0.36\,\lambda_0 \times 0.48\,\lambda_0 \times 0.13\,\lambda_0$, where λ_0 denotes the wavelength in free-space at the center frequency. A wide impedance bandwidth of 64.8% (17.1 GHz – 33.5 GHz) is achieved for SWR ≤ 2, in which the antenna gain varies from 5.9 dBi to 8.8 dBi. Besides, a consistent unidirectional radiation pattern can be observed across the operating frequency band. In the sequel, the same antenna is aggregated into an 8-element linear array which is fed by a designated 8-way SICL network. Finally, an active simulation has been performed to verify the ability of the array in beam scanning.

Index Terms—ME dipole; millimeter-wave; compact antenna; wide bandwidth; beam scanning.

I. INTRODUCTION

THE enormous development of wireless communication systems, including radar, telecommunication systems, satellite communication systems, radio and television broadcasting, and internet of everything (IoE) systems, has been driving the breakthrough in antenna design to exploit the potential of future wireless communications thoroughly [1]. Nevertheless, it is strenuous to overcome the trade-off between the requirements of modern antennas, encapsulated as wide operational bandwidth, small size, low profile, stable gain, high efficiency, and easy integration with front ends [1], [2].

The magneto-electric (ME) dipole antenna is well-known for its wide bandwidth, stable gain, high front-to-back ratio, low cross-polarization level, and symmetrical radiation patterns in E- and H-planes [3]. However, it has a high profile caused by the vertically oriented shorted patch. Meanwhile, the current path should be half-wavelength for a typical electric or magnetic dipole to be in resonance, explaining why the height of a conventional ME dipole is considered quarter-wavelength [3].

Indeed, a few attempts have been dedicated to reducing the size of the ME dipoles, and their main approaches can be summarized as increasing the current path length to reduce the resonant frequency. For instance, the electric dipole patch is truncated by several transverse open-ended slots to reduce the size of the ME dipole [4]. Besides, the profile of the ME dipoles can be reduced by either folding the vertically oriented shorted patch [5] or replacing the shorted patch with a triangular-shaped loop antenna [6]. Not to mention, a ME dipole is miniaturized by adopting magnetic metamaterial between the shorted patch and the Γ-shaped probe [7]. Last but not least, it is reported that a volume size reduction of 48% can be obtained by increasing the effective permeability of the substrate by adding some split-ring resonators. Nonetheless, most of the reported size reduction techniques applied to the ME dipole antennas would commonly lead to gain instability, narrower impedance bandwidth, and more complex structures. Consequently, a practical approach for miniaturizing the ME dipole without distorting other radiation properties is still an open problem.

In recent years, electromagnetic metasurfaces, a subset of metamaterials, have been drawing attention due to their non-existent properties and artificially achievable response functions [8]. An early design pioneered the exploitation of reactive impedance surface (RIS) to realize optimization of bandwidth and antenna miniaturization at the telemetry frequency range, with the benefit of preserving other radiation properties [2]. Latterly, the RIS structure was first applied to a fractal ME dipole with the second-order Minikowski structured patches to achieve a size reduction of 51% and a wide

Tsz-Ming Wong is with the State Key Laboratory of Terahertz and Millimeter Waves, Department of Electrical Engineering, City University of Hong Kong, Hong Kong SAR 999077, China, and also with the City University of Hong Kong Shenzhen Research Institute, Shenzhen 518057, China (e-mail: tmwong34-c@my.cityu.edu.hk).

Kwai-Man Luk is with the State Key Laboratory of Terahertz and Millimeter Waves, Department of Electrical Engineering, City University of Hong Kong, Hong Kong SAR 999077, China, and also with the City University of Hong Kong Shenzhen Research Institute, Shenzhen 518057, China (e-mail: eekmluk@cityu.edu.hk).

Kin-Fai Tong is with the Department of Electronic and Electrical Engineering, University College London, Torrington Place, United Kingdom (email: k.tong@ucl.ac.uk).

bandwidth of 39.7% [9].

Meanwhile, a planar and simple antenna structure is preferred for mounting or packaging an antenna on a platform. Notwithstanding, most of the reported ME dipoles require either a complicated design of an electric dipole patch or a quarter-wavelength shorted patch, which substantially increases the production cost and fabrication complexity as it is duplicated in a massive array at higher frequencies. A simple coaxially fed ME dipole without the quarter-wavelength shorted patch was proposed [10]. It stated that the magnetic dipole mode could be activated by exciting the gap slot between the two planar electric dipole patches [10]. After removing the traditional quarter-wavelength patch, the new design can reduce the height of the ME dipole to $0.164\,\lambda_0$, where λ_0 denotes the free-space wavelength at the center frequency. Notably, over the relatively wide impedance bandwidth of 41%, a high and stable gain of 7.9 dBi to 9.7 dBi can still be achieved. Following the ideas in [10], the previous model is modified into an aperture-coupled low-profile ME dipole antenna [11]. The height of the proposed ME dipole is further reduced to $0.12\,\lambda_0$, whereas the impedance bandwidth has significantly declined to 29.1%. Being attracted by its low profile, simple structure, and easy integration with front ends, several modifications are presented in this literature.

The main contribution of this literature is threefold and listed below:

1) A wideband aperture-coupled via-free ME dipole antenna is designed afresh after [11]. Instead of circumventing the quarter-wavelength shorted patch by the gap of the electric dipole, this work has proposed to etch a half-wavelength radiating slot on the ground plane to activate the magnetic dipole mode. Besides, a substrate integrated coaxial line (SICL) feed network is deployed to excite the antenna. Compared to the printed ridge gap waveguide (PRGW) [12] and the substrate integrated waveguides (SIW) feed networks [13], SICL has the advantage of a more compact and flexible structure. In addition, the SICL can reduce the back radiation caused by the aperture slot and incurs less radiation loss than the microstrip lines (MSL) [14].

2) The reactive impedance surface (RIS) [2] is then designed according to the normalized input impedance of the proposed antenna to optimize the impedance bandwidth while miniaturizing the antenna size, in terms of wavelength, by reducing the operating frequency. For convenience, we will use *Ant. 1* and *Ant. 2* to label the via-free ME dipole antenna without and with the RIS, respectively, for the rest of the paper.

3) An 8-element linear antenna array fed by an 8-way parallel SICL feed structure is analyzed and measured to verify the performances of the proposed via-free ME dipole antenna. Eventually, a potential beam scanning ability is demonstrated by performing an active simulation.

II. WIDEBAND VIA-FREE ME DIPOLE ANTENNA

A. Antenna Geometry

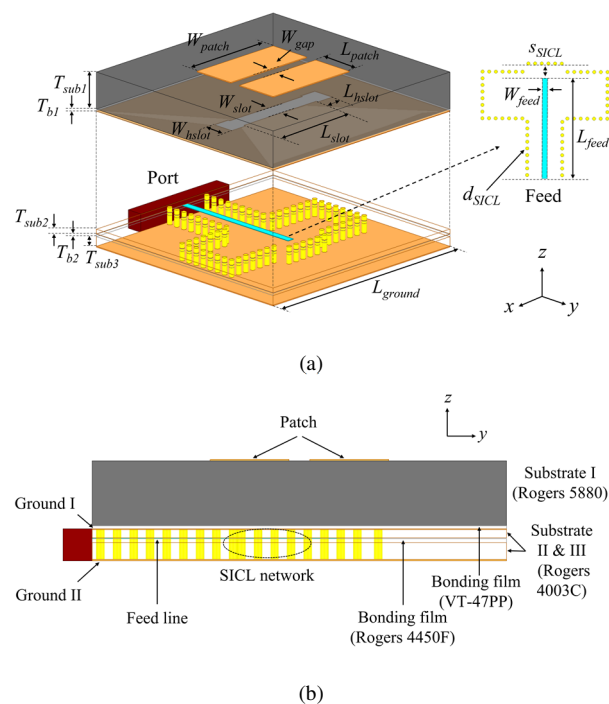The geometry of *Ant. 1* fed by a SICL network is depicted in

Fig. 1. Geometry of the proposed via-free ME dipole antenna (*Ant. 1*) fed by the network of resonant aperture slot and SICL. (a) Perspective view, and (b) side view.

TABLE I
KEY DIMENSIONS OF *ANT. 1* IN FIG. 1

Parameter	L_{ground}	T_{sub1}	T_{sub2}	T_{sub3}
Value (mm)	10 ($0.9\,\lambda_0$)	1.575 ($0.14\,\lambda_0$)	0.203 ($0.018\,\lambda_0$)	0.406 ($0.037\,\lambda_0$)
Parameter	L_{patch}	W_{patch}	W_{gap}	T_{b1}
Value (mm)	1.9 ($0.17\,\lambda_0$)	4.3 ($0.39\,\lambda_0$)	0.5 ($0.045\,\lambda_0$)	0.07 ($0.0063\lambda_0$)
Parameter	T_{b2}	W_{slot}	L_{slot}	W_{hslot}
Value (mm)	0.1 ($0.009\,\lambda_0$)	0.8 ($0.072\,\lambda_0$)	4.1 ($0.37\,\lambda_0$)	1 ($0.09\,\lambda_0$)
Parameter	L_{hslot}	W_{feed}	L_{feed}	s_{SICL}
Value (mm)	0.8 ($0.072\,\lambda_0$)	0.3 ($0.027\,\lambda_0$)	6 ($0.54\,\lambda_0$)	0.8 ($0.072\,\lambda_0$)
Parameter	d_{SICL}			
Value (mm)	0.2 ($0.018\,\lambda_0$)			

λ_0: wavelength in free-space at the center frequency of 27 GHz.

Fig. 1, while the detailed dimensions are described in Table I. Firstly, two rectangular metallic patches are separated by a narrow gap of W_{gap}. Each patch has dimensions of L_{patch} x W_{patch}, implying that the length of each patch (L_{patch}) is about one-quarter-wavelength. Altogether, two patches operate as a planar electric dipole along the horizontal *xoy*-plane. Whilst *Ant. 1* has three layers of substrate. A piece of Rogers 5880 material (ε_r = 2.2, tanδ = 0.0009 at 10 GHz) with a thickness of T_{sub1} is assigned as Substrate I to support the patches. Below there are Substrate II and Substrate III (Rogers 4003C, ε_r = 3.55, tanδ = 0.0027 at 10 GHz) with the thickness of T_{sub2} and T_{sub3} respectively, and the two substrates integrate with the SICL to form the feed layer. Metallic vias of SICL are vertically placed with a periodicity of 2 x d_{SICL} at a fixed distance of s_{SICL} away from the feed line and aperture slot to shield a planar

coaxial line structure, where d_{SICL} denotes the diameter of the metallic vias. Notice that Substrate I is thicker than the lower feed layer to ensure better radiation efficiency. Moreover, thinner material with higher relative permittivity is selected to compose the feed layer to minimize the spurious radiation in the feedline.

Bonding films are deployed to ensure a good electrical connection between conduction layers. The first bonding film (VT-47PP, $\varepsilon_r = 4.3$, $\tan\delta = 0.018$ at 1 GHz) with a thickness of T_{b1} is sandwiched between Substrate I and Ground I. While the second bonding film (Rogers 4450F, $\varepsilon_r = 3.5$, $\tan\delta = 0.004$ at 10 GHz) with a thickness of T_{b2} is applied to bond Substrate II and Substrate III together. Apart from this, two different metal thickness is considered. Thicker metal cladding of 35 μm (1 oz) is assigned to the exposing metal, corresponding to the two metallic patches and the bottom Ground II. Meanwhile, the thickness of Ground I is set as 18 μm (1/2 oz). All the mentioned substrates, ground planes, and bonding films have the identical size of L_{ground} x L_{ground}.

Furthermore, an H-shaped aperture is deployed in our design, which is etched in Ground I. As stated in [15]-[16], the H-shaped aperture features higher resonance impedance such that it can support better coupling than that of the ordinary rectangular and bowtie-shaped apertures of the same length. As a result, the H-shaped aperture is selected to reduce the spurious back radiation created from the aperture slot and shorten its length to nearly a half wavelength, equivalents to the desired element spacing for minimizing the side lobes of an antenna array when performing beam steering. Finally, the antenna is analyzed using the full-wave solver ANSYS HFSS.

B. Principle of Operation

Recapping the working principles of a ME dipole antenna, it constitutes a pair of complementary electric and magnetic dipoles [3]. In general, the two dipole sources are arranged in an orthogonal manner. It is well-known that the radiation pattern of an electric dipole appears as an "inverted-8" in the E-plane and an omnidirectional pattern in the H-plane, whereas the radiation pattern of a magnetic dipole is reciprocal to that of the electric dipole in different planes. It has been proven that when both dipole sources are excited simultaneously with identical amplitude and phase, the antenna can exhibit identical symmetric cardioid-alike radiation patterns in both E- and H-planes with low backlobe radiation. Apart from that, the ME dipole antenna features other excellent radiation properties, including stable radiation patterns, consistent high gain over a wide bandwidth, and low cross-polarization level.

Inspired by the concept of the ME dipole and the previous literature [10]-[11], a novel idea of exciting the magnetic dipole mode via a half-wavelength resonant H-shaped aperture slot in the ground plane is presented in this literature. The dimensions of the H-shaped aperture slot are designed to radiate and excite the magnetic dipole mode for attaining the features of a typical ME dipole antenna. By fixing the horizontal length ($L_{slot} + 2$ x L_{hslot}) of the aperture slot to be about half-wavelength in free-space at the center frequency, the width of the aperture slot (W_{slot}) is optimized for achieving the best impedance
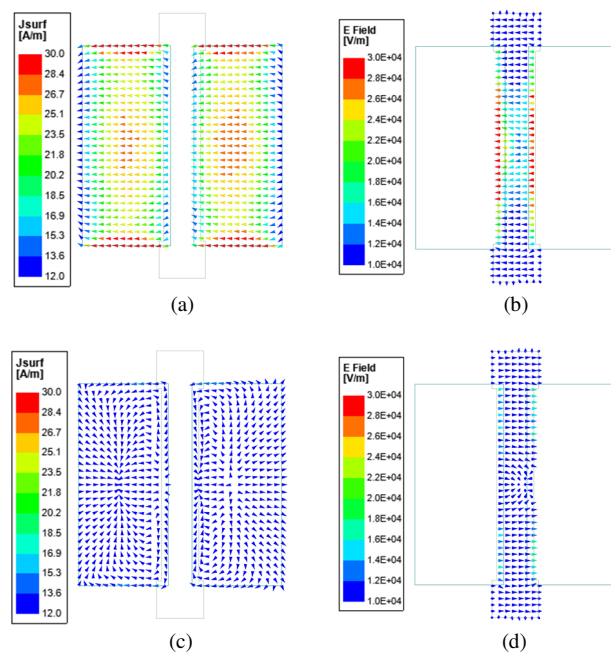

Fig. 2. Current distribution and E-field distribution at 27 GHz of the proposed via-free ME dipole antenna. (a) $t = 0$, current distribution, (b) $t = 19T/24$, E-field distribution, (c) $t = T/4$, current distribution, (d) $t = T/24$, E-field distribution.

matching. After performing the parametric studies of all the variables, W_{slot} is determined as the dominant factor of controlling the upper resonant frequency, which is contributed by the magnetic dipole mode. In order to provide a more comprehensive insight into the working principle of the designed antenna, the current distribution on the bottom surface of the patches and the E-field distribution in the H-shaped aperture slot at 27 GHz are depicted in Fig. 2. The phase difference θ_d due to the thickness of Substrate I is considered, which equals 1.30 rad ($\sim 5T/24$) and is calculated as:

$$\theta_d(\,in\ radian) = kd = \left(\frac{2\pi}{\lambda}\right)(d) \tag{1}$$

, where T is the oscillation's period, λ represents the wavelength in the dielectric and d denotes the path difference of T_{sub1} ($0.14\lambda_0$).

The current intensity near the side edge of patches and the E-field at the horizontal portion of the aperture slot are observed to attain maximum value at time $t = 0$ and $19T/24$ respectively. In contrast, they are minimum at time $t = T/4$ and $T/24$ respectively. As a result, we have successfully verified that the electric and magnetic dipole modes are excited in-phase at the patch layer. This explains why the proposed antenna can operate as a complementary antenna even though no quarter-wavelength shorted patch is deployed.

On the other hand, the previous claim that the magnetic resonant is mainly determined by W_{slot} is proven by plotting the dependence of input impedance on W_{slot}, as shown in Fig. 3. Similar to the ordinary ME dipole antenna [3], two local maxima are observed in the $Re\{Z_{11}\}$ plot within the operational frequency band. When there is a drop in the value of W_{slot}, the higher resonant frequency at 30 GHz shifts to a lower frequency, whereas the lower resonant frequency at 19 GHz is

This article has been accepted for publication in IEEE Transactions on Antennas and Propagation. This is the author's version which has not been fully edited and content may change prior to final publication. Citation information: DOI 10.1109/TAP.2023.3299631

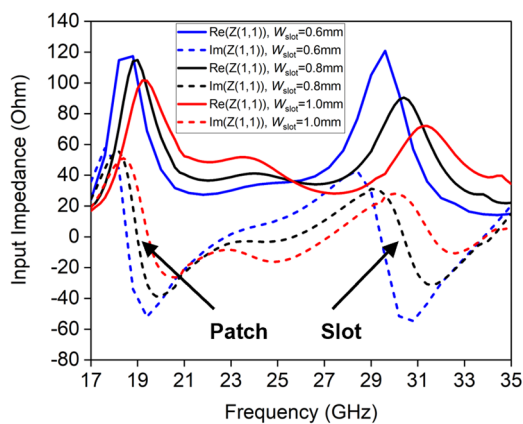> REPLACE THIS LINE WITH YOUR PAPER IDENTIFICATION NUMBER (DOUBLE-CLICK HERE TO EDIT) <   4

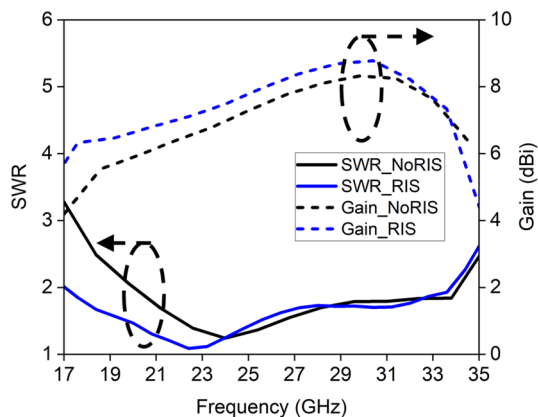Fig. 3. Impedance response with the width of aperture slot W_{slot}.

Fig. 4. Simulated gain and SWR of the proposed via-free ME dipole antenna before and after loading the structure of RIS.

relatively invariant to the changes of W_{slot}. Finally, the value of W_{slot} is chosen to be 0.8 mm for optimizing the radiation properties of the proposed antenna, including the SWR bandwidth, gain bandwidth, and front-to-back ratio.

C. Simulation Results

To evaluate the performance of *Ant. 1*, various simulations are conducted. First, the simulated SWR and gain of *Ant. 1* are shown in Fig. 4. Although the designed antenna has not implemented the quarter-wavelength shorted patch for imitating the magnetic dipole, it can still exhibit wide impedance bandwidth (SWR ≤ 2) of 52.1% from 20 GHz to 34.1 GHz, which has significantly improved the impedance matching performance when comparing with the model stated in [11]. Not to mention, the designed antenna can support a stable high gain from 5.9 dBi to 8.3 dBi (7.1 dBi ± 1.2 dBi) across the operating frequency band. Whilst in Fig. 5, the simulated radiation patterns of E-plane and H-plane at 23 GHz, 27 GHz, and 31 GHz are illustrated. Symmetric and directional E- and H-plane radiation patterns can be realized in the wide frequency band. Moreover, a low cross-polarization level of less than -31 dB and a low backlobe radiation level of less than -17.9 dB can be achieved at 23 GHz and 27 GHz. Although the backlobe radiation level is increased to -11 dB at 31 GHz, a directional radiation pattern with low cross-polarization level of -27 dB can still be obtained.
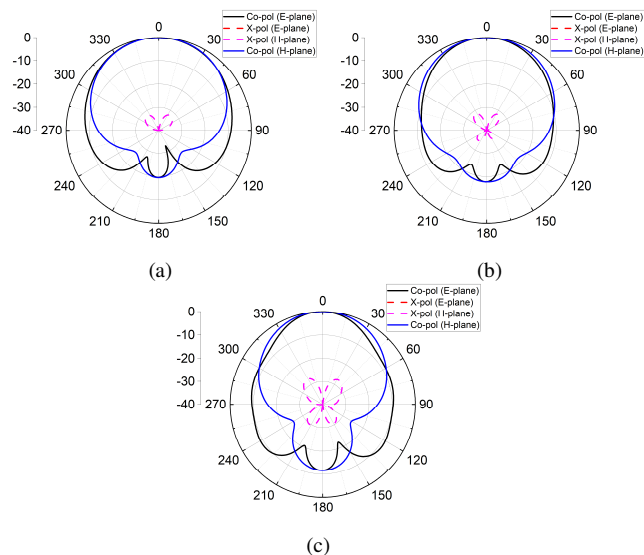

Fig. 5. Simulated normalized radiation pattern of *Ant. 1* at (a) 23 GHz, (b) 27 GHz, and (c) 31 GHz.

To summarize, the designed antenna utilizes the resonant H-shaped aperture slot to replace the conventional quarter-wavelength shorted patch for exciting the magnetic dipole mode at high resonance. This novel idea helps to relieve the height constraint of a typical ME dipole such that a low-profile and via-free radiating structure with a projected area of (2 x L_{patch} + W_{gap}) x (L_{slot} + 2 x L_{hslot}) x T_{sub1} = 0.39 λ_0 x 0.51 λ_0 x 0.14 λ_0 can be realized. Despite its relatively simple structure, it features excellent radiation properties such as wide bandwidth, consistent directional radiation pattern, low cross-polarization level, and high gain. The following section will discuss detailed procedures for designing *Ant. 2*.

III. MINIATURIZED VIA-FREE ME DIPOLE ANTENNA ON RIS

A. Procedures of Designing Capacitive RIS Structure

RIS is a metal-backed dielectric substrate with two-dimensional metallic patches periodically printed on its surface [2]. It is commonly known that the reflection phase of a perfect electric conductor (PEC) and a perfect magnetic conductor (PMC) is 180° and 0° respectively, which can be interpreted as a transmission line terminated by a short circuit and open circuit accordingly [17]. In contrast, RIS is a purely reactive surface that can generalize both PEC and PMC by realizing arbitrary reflection phases ranging from −180° to 180°.

Indeed, both PEC and PMC surfaces suffer from severe loss of near-field electromagnetic energy due to their strong coupling with the elementary source, causing them not to be the ideal ground plane of the antenna. On the other hand, RIS with a specific surface reactance is reported to realize bandwidth enhancement and antenna miniaturization as the adverse effects caused by a traditional ground plane can be minimized [2]. Herein, the adverse effects refer to the interaction between the antenna source and its current image, which causes the undesired storage of electromagnetic energy in the near field and an increase of radiation Q of the antenna.
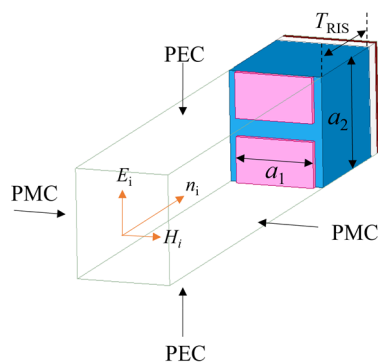
Fig. 6. Unit cell of the RIS surrounded by PEC-PMC boundaries in the x-y directions and illuminated by the normal incident plane wave.

Most of the image current has been demonstrated to focus at the image point on an arbitrary impedance surface when the impedance surface has real surface impedance values [2]. Nevertheless, the image current can be sinusoidally distributed when the impedance surface is entirely reactive, significantly reducing the interaction between the source and its image [2]. It can also guarantee a unity magnitude of the reflection coefficient for total power reflection. Therefore, the surface impedance of RIS is assigned as

$$\eta = jb \qquad (2)$$

Theoretically, when the normalized surface impedance (b/η_0) of RIS is properly deliberated, where η_0 denotes the vacuum wave impedance, the energy stored in the elementary source can be compensated by the energy stored in its image. This allows the resonance of an inductively (or capacitively) loaded antenna to be shifted to a lower frequency when its image source can store the electric (or magnetic) energy, which eventually reduces the size of the antenna, in terms of wavelength, and improves the impedance matching.

Fig. 6 describes a RIS unit cell illuminated by a normal incident plane wave. While the PMC and PEC walls are established perpendicular to the incident magnetic field and electric field respectively to form the periodic boundary conditions, which can reduce the simulation complexity yet provide an accurate approximation of the RIS behavior. The substrate thickness (T_{RIS}), the dimensions (a_1 x a_1), and the periodicity (a_2) of the RIS square patches are tuned to offer the desired surface impedance of RIS. Recapping the input impedance of *Ant. 1* in Fig. 3, the antenna is inductive below 19 GHz when W_{slot} = 0.8 mm. According to the design theory stated previously, the RIS structure should be designed as capacitive below this frequency such that a lower antenna resonance frequency can be achieved for size reduction. Therefore, the variables T_{RIS}, a_1, and a_2 are adjusted to optimize the capacitive region of RIS to match with the frequency band that the antenna is inductive, and the finalized values are T_{RIS} = 0.787 mm, a_1 = 0.5 mm, and a_2 = 0.6 mm.

The normalized surface impedance of the proposed RIS structure is presented in Fig. 7, and its resonant frequency appears at 10.5 GHz. As stated in [2] and [18], the RIS structure can be interpreted as a parallel LC circuit, such that it behaves as an open circuit at the resonant frequency. Additionally, the
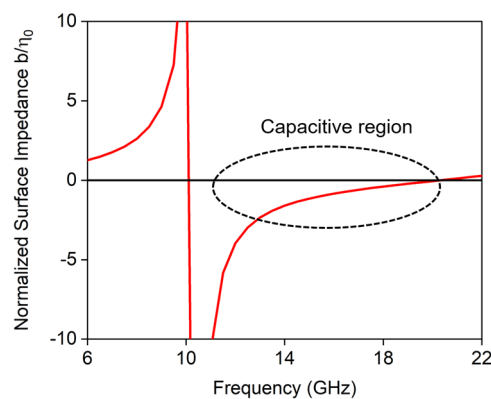

Fig. 7. Normalized surface impedance of the proposed RIS structure with T_{RIS} = 0.787 mm, a_1 = 0.5 mm, and a_2 = 0.6 mm.
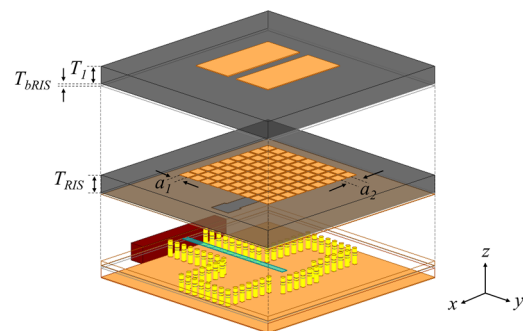

Fig. 8. Configuration of the proposed via-free ME dipole antenna loaded with RIS structure (*Ant. 2*). New antenna parameters: T_1 = 0.787 mm, T_{bRIS} = 0.1 mm, T_{RIS} = 0.787 mm, a_1 = 0.5 mm, and a_2 = 0.6 mm.

parallel LC circuit becomes inductive and capacitive when the operating frequency is below and above its resonant frequency respectively. Hence, the proposed RIS structure is designed as capacitive from 10.5 GHz to 20.3 GHz. Since the antenna is inductive below 19 GHz, the magnetic energy stored in the near-field of the designed via-free ME dipole can be compensated by the electric energy stored in RIS within the frequency range of 10.5 GHz to 19 GHz. Eventually, a lower resonant frequency of the antenna can be realized for antenna miniaturization, while minimizing the mutual coupling between the source and image current by RIS can lead to bandwidth enhancement.

B. Antenna Geometry

To evaluate the merits of the RIS structure, a 9 × 9 array of the proposed RIS unit is loaded into *Ant. 1* to become *Ant. 2*. As reflected in Fig. 8, *Ant. 2* shares the same layer structure as *Ant. 1*, except for loading the array of RIS into Substrate I, such that $T_1 + T_{bRIS} + T_{RIS} \approx T_{sub1}$. Here, T_{bRIS} denotes the thickness of the bonding film (Rogers 4450F, ε_r = 3.5, tanδ = 0.004 at 10 GHz) being added between the upper half of Substrate I and the top surface of the RIS. Besides, L_{slot} is adjusted to 4.2 mm to optimize the antenna performance of *Ant. 2*. Most importantly, neither the profile nor the structure shape is affected by loading the RIS structure. For clarity, the key dimensions of *Ant. 2* are summarized in Table II.

TABLE II
KEY DIMENSIONS OF *ANT. 2* IN FIG. 8

Parameter	L_{ground}	T_{sub2}	T_{sub3}	L_{patch}
Value	10	0.203	0.406	1.9
(mm)	$(0.83\,\lambda_0)$	$(0.0169\,\lambda_0)$	$(0.034\,\lambda_0)$	$(0.16\,\lambda_0)$
Parameter	W_{patch}	W_{gap}	T_{b1}	T_{b2}
Value	4.3	0.5	0.07	0.1
(mm)	$(0.36\,\lambda_0)$	$(0.042\,\lambda_0)$	$(0.0058\lambda_0)$	$(0.0083\lambda_0)$
Parameter	W_{slot}	L_{slot}	W_{hslot}	L_{hslot}
Value	0.8	4.2	1	0.8
(mm)	$(0.072\,\lambda_0)$	$(0.35\,\lambda_0)$	$(0.083\,\lambda_0)$	$(0.067\,\lambda_0)$
Parameter	W_{feed}	L_{feed}	s_{SICL}	d_{SICL}
Value	0.3	6	0.8	0.2
(mm)	$(0.025\,\lambda_0)$	$(0.5\,\lambda_0)$	$(0.067\,\lambda_0)$	$(0.016\,\lambda_0)$
Parameter	T_1	T_{bRIS}	T_{RIS}	a_1
Value	0.787	0.1	0.787	0.5
(mm)	$(0.066\,\lambda_0)$	$(0.0083\,\lambda_0)$	$(0.066\,\lambda_0)$	$(0.042\,\lambda_0)$
Parameter	a_2			
Value	0.6			
(mm)	$(0.05\,\lambda_0)$			

λ_0: wavelength in free-space at the center frequency of 25 GHz.

C. Simulation Results

In Fig. 4, the simulated SWR and gain of *Ant. 1* and *Ant. 2* are compared. As discussed, the RIS structure is designed to be capacitive to compensate for the magnetic energy stored in the near-field of *Ant. 1*, which can eventually reduce the operating frequencies for achieving antenna miniaturization. Consequently, the center frequency f_0 of *Ant. 2* has shifted from 27 GHz to 25 GHz, implying that the final dimensions of *Ant. 2* excluding RIS become $0.36\,\lambda_0$ x $0.48\,\lambda_0$ x $0.13\,\lambda_0$. This yields a size reduction of 19% from the previous *Ant. 1* when the RIS structure is not counting towards the size calculation. The projected area of the antenna, including the RIS, is (a_1+8a_2) x $(L_{slot} + 2$ x $L_{hslot})$ x $(T_1 + T_{bRIS} + T_{RIS}) = 0.44\,\lambda_0$ x $0.48\,\lambda_0$ x $0.13\,\lambda_0$.

Since the magnetic resonance of the proposed antenna at a higher frequency is excited by the resonant aperture slot, which is positioned below the RIS structure, the deployment of the RIS structure will only shift the electric resonance generated by the metallic patches to a lower frequency. Hence, the impedance bandwidth of *Ant. 2* can be further increased from 52.1% to 64.8% (17.1 GHz – 33.5 GHz) for SWR ≤ 2. Meanwhile, after loading with the RIS, the antenna gain is slightly enhanced and varies between 5.9 dBi and 8.8 dBi (7.4 dBi ± 1.4 dBi) across the operating frequency band. This happens as the RIS structure allows the image current to be sinusoidally distributed over a larger effective area rather than focused on the image position [2], [9].

Table III compares *Ant. 2* with other reported ME dipole with similar structures, such that all the listed designs are not using the quarter-wavelength shorted patch to excite the magnetic dipole mode. By considering the model with equivalent excitation approach [11], although the proposed antenna features more compact size, it can obtain wider bandwidth and higher realized gain. The antenna gain enhancement is mainly caused by an increase in the effective area due to the RIS structure.

Finally, the simulated radiation patterns of the proposed

TABLE III
COMPARISON BETWEEN THE PROPOSED AND REPORTED ME DIPOLE ANTENNAS
WITHOUT THE QUARTER-WAVELENGTH SHORTED PATCH

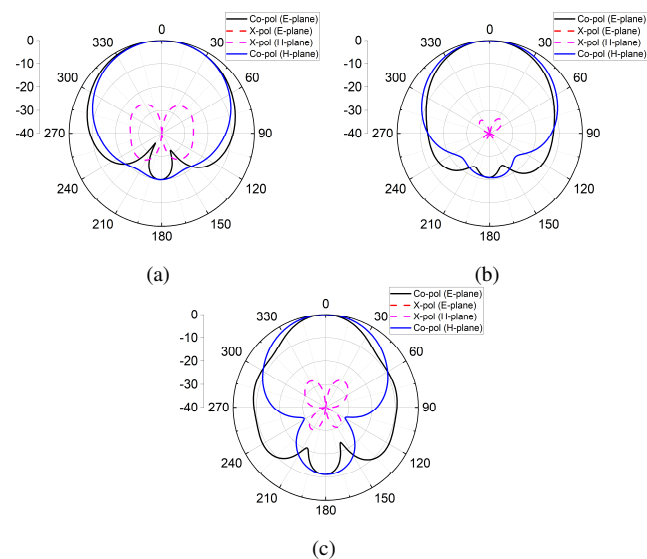| Antenna model	Coupling Methods	f_0 (GHz)	Projected Area	Impedance Bandwidth	Max. Realized Gain (dBi)
[10]	Coaxial probe	2.34	$0.48\,\lambda_0$ x $0.47\,\lambda_0$ x $0.16\,\lambda_0$	41.0%	9.7
[11]	Aperture	27.5	$0.45\,\lambda_0$ x $0.60\,\lambda_0$ x $0.12\,\lambda_0$	29.1%	8.3
This work	Aperture	25	$0.44\,\lambda_0$ x $0.48\,\lambda_0$ x $0.13\,\lambda_0$	64.8%*	8.8*

*Simulated results.

(a)   (b)

(c)

Fig. 9. Simulated normalized radiation pattern of the proposed via-free ME dipole antenna loaded with RIS structure at (a) 18 GHz, (b) 25 GHz, and (c) 31 GHz.

antenna at 18 GHz, 25 GHz, and 31 GHz are illustrated in Fig. 9. As depicted, the directional radiation pattern can still be preserved for wideband even after achieving antenna miniaturization by loading the RIS structure. Apart from attaining a low cross-polarization level below -25.5 dB, it is worth mentioning that the back radiation level at the center frequency f_0 can also be reduced from -18 dB to -22 dB after the deployment of the RIS structure. All in all, the approach of loading RIS to the proposed via-free ME dipole antenna is proven to achieve size miniaturization and bandwidth enhancement with minimal effects on other radiation properties.

IV. COMPACT ME DIPOLE ANTENNA ARRAY

A. Geometry of Proposed 8-Element Array with SICL Feed Network

To further demonstrate the performance of the proposed antenna, *Ant. 2* is aggregated into an 8-element linear array with an inter-element spacing of $s = 6$ mm along the x-axis, which is equivalent to $0.5\,\lambda_0$ at 25 GHz as depicted in Fig. 10. The changed antenna parameters for performance optimization are

This article has been accepted for publication in IEEE Transactions on Antennas and Propagation. This is the author's version which has not been fully edited and content may change prior to final publication. Citation information: DOI 10.1109/TAP.2023.3299631

> REPLACE THIS LINE WITH YOUR PAPER IDENTIFICATION NUMBER (DOUBLE-CLICK HERE TO EDIT) <   7
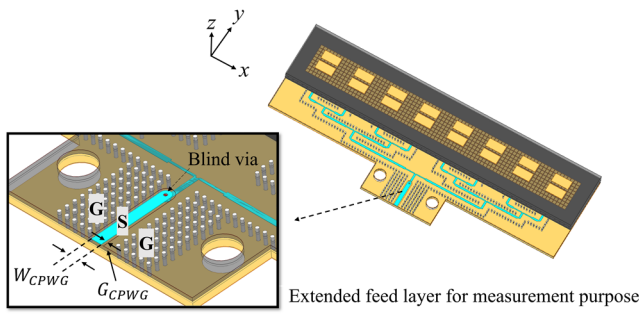
Fig. 10. Configuration of the proposed 8-element ME dipole antenna array fed by the SICL network. A ground-signal-ground (GSG) feed structure is realized by the coplanar waveguide with ground (CPWG). Changed antenna parameters: $L_{patch} = 1.5$ mm, $W_{patch} = 3$ mm, $L_{slot} = 4.1$ mm, $W_{hslot} = 1.3$ mm.
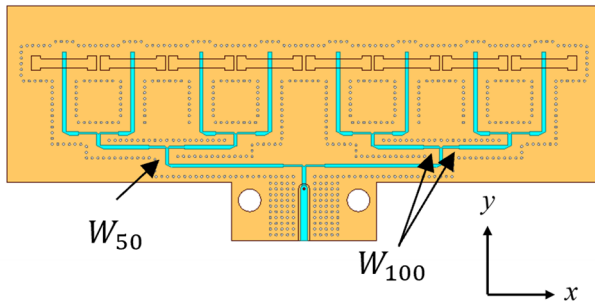

Fig. 11. Configuration of the proposed SICL feed network.

listed in the captions of Fig. 10. Specifically, the patch size is tuned to match the capacitive region of the RIS structure with the decreased inductive region of the array.

Then, the antenna array is attached to an 8-way SICL power divider that consists of three stages of parallel power dividers to distribute power evenly to the eight ports of the linear array. As mentioned in Section II, Substrate II and Substrate III complement the SICL network to establish the feed layer of the antenna. Additionally, the feed layer is further extended in the y-direction and drilled with two screw holes to hold the end launch connector. To apply the SICL feed network, a coplanar waveguide with ground (CPWG) is mounted on Ground I to facilitate an electrical connection between the signal pin of the waveguide connector and the SICL through a blind via, as indicated in Fig. 10. The signal feed width (W_{CPWG}) is set as 0.65 mm, while the gap (G_{CPWG}) is 0.15 mm. The projected area of the proposed array is $(a_1 + 8a_2)$ x $s = 0.44\ \lambda_0$ x $0.5\ \lambda_0$.

B. Design of SICL Feed Network

As stated in [19]-[20], the full-corporate feeding structures such as the stripline (SL), MSL, and coplanar waveguide are often suffering from high radiation loss and severe cross-polarization level in the millimeter wave band. In contrast, SIW is another type of substrate-integrated feeding network that features low insertion and radiation loss, whereas it exhibits narrow operating bandwidth due to the cut-off frequency of the dominant and higher-order modes. Therefore, the compact, wideband, and highly efficient SICL feed network can serve as a good substitution for the mentioned approaches and is applied to excite the antenna in this literature.
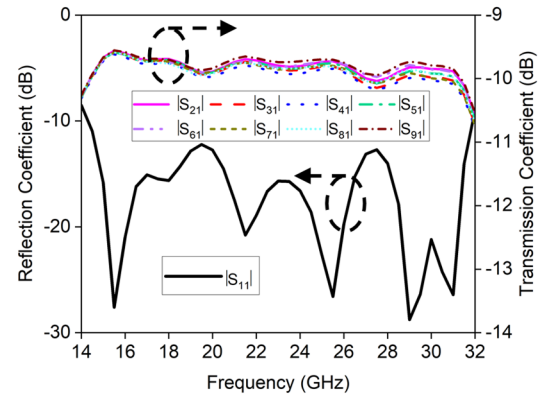

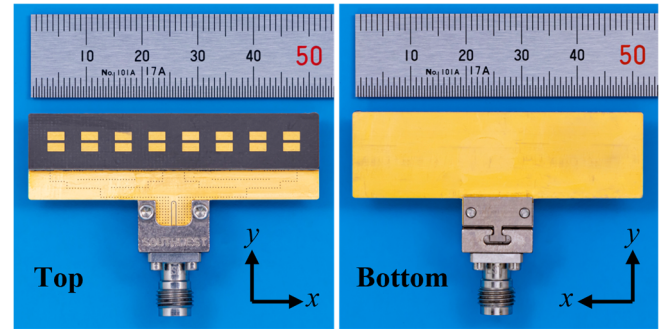Fig. 12. Reflection and transmission coefficients of the proposed SICL feed network.

Fig. 13. Fabricated prototype of the proposed linear array.

The top view of the SICL feed structure is demonstrated in Fig. 11. To build an 8-way power divider, three stages of parallel power dividers are deployed to distribute power evenly. Each pair of power dividers consist of one 50 Ω and two 100 Ω transmission lines, and their line widths are $W_{50} = 0.3$ mm and $W_{100} = 0.13$ mm respectively. To establish the SICL structure, the signal feed line of the SICL is wedged between two metal-backed dielectric substrates, which corresponds to Substrate II and Substrate III as shown in Fig. 1.

To verify the performance of the SICL feed network, the reflection and transmission coefficients of the proposed SICL feed structure are illustrated in Fig. 12. A return loss of higher than 12.2 dB from 14.6 GHz to 31.7 GHz can be realized, while the in-band variation of the insertion losses is observed to be within 0.7 dB.

C. Experimental Results

After designing a wideband and low-loss SICL feed network, we apply it to the proposed via-free ME dipole antenna elements, and the fabricated array prototype is depicted in Fig. 13. To measure the SWR of the linear array, an Agilent vector network analyzer E8361A was selected. While a compact range far-field measurement system was used to measure the radiation performance of the linear array.

Both the measured SWR and gain agree well with the simulated results, as shown in Fig. 14 and Fig. 15, such that an overlapped bandwidth of 48.9% is realized for SWR ≤ 2 from 18.7 GHz to 30.8 GHz, while the measured gain is up to 13.8 dBi. The deviation of the measured SWR and gain from the
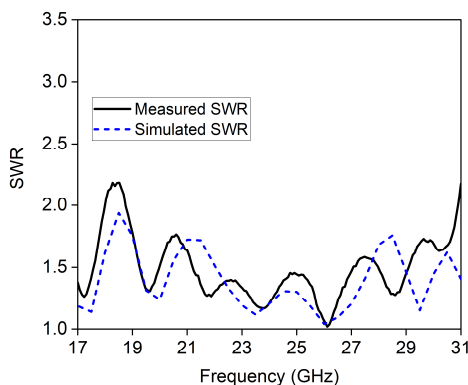
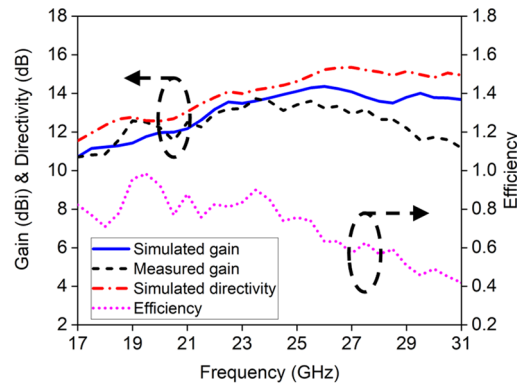Fig. 14. Measured and simulated SWR of the proposed linear array.

Fig. 15. Measured and simulated gain, directivity and efficiency of the proposed linear array.

simulated results at high frequencies is due to the more substantial in-band variation of insertion losses caused by the SICL. In addition, the estimated efficiency of the proposed linear array is computed by comparing the simulated directivity with the measured gain in Fig. 15. The maximum estimated

efficiency is 98%, whereas the average efficiency is 72% over the operating frequency band. Notice that a drop in efficiency at high frequencies is mainly due to the imperfect electrical connection between the signal pin of the waveguide connector and the SICL feed network. This impedance mismatch between the coaxial cable and the feed network increases with the frequency, gradually reducing the efficiency at higher frequency bands.

Fig. 16 portrays the measured and simulated normalized radiation patterns of the linear array at 20 GHz, 25 GHz, and 30 GHz. Although the measured and simulated radiation patterns are slightly deflected from each other in the E-plane (*yoz*-plane) due to the undesired reflection from the end-launched connector, the measured radiation pattern conforms well to the simulated results in the H-plane (*xoz*-plane). The back radiation is maintained below -19.8 dB for all scenarios, and the sidelobe level in H-plane is less than -13.2 dB. Last but not least, the cross-polarization level of the proposed array is below -18.4 dB.

D. Beam Scanning Performance

Beam scanning is one of the most crucial millimeter wave band applications, and it will be discussed in the remaining section. Although the proposed antenna is initially designed for providing a fixed beam direction, its beam scanning capability can still be evaluated by neglecting the SICL feed network and executing the active simulation using the full-wave solver ANYSIS HFSS. The design procedures will be like designing a traditional uniform phased array, such that all elements are excited with identical amplitudes and progressive phase difference. As demonstrated in Fig. 17, the proposed antenna can support a wide scanning range of 55° with 3-dB scan losses below 25 GHz, whereas the scanning angle is slightly reduced to 45° with an increased sidelobe at 31 GHz. The sidelobe levels at 20 GHz, 25 GHz and 31 GHz are below -12.5 dB, -
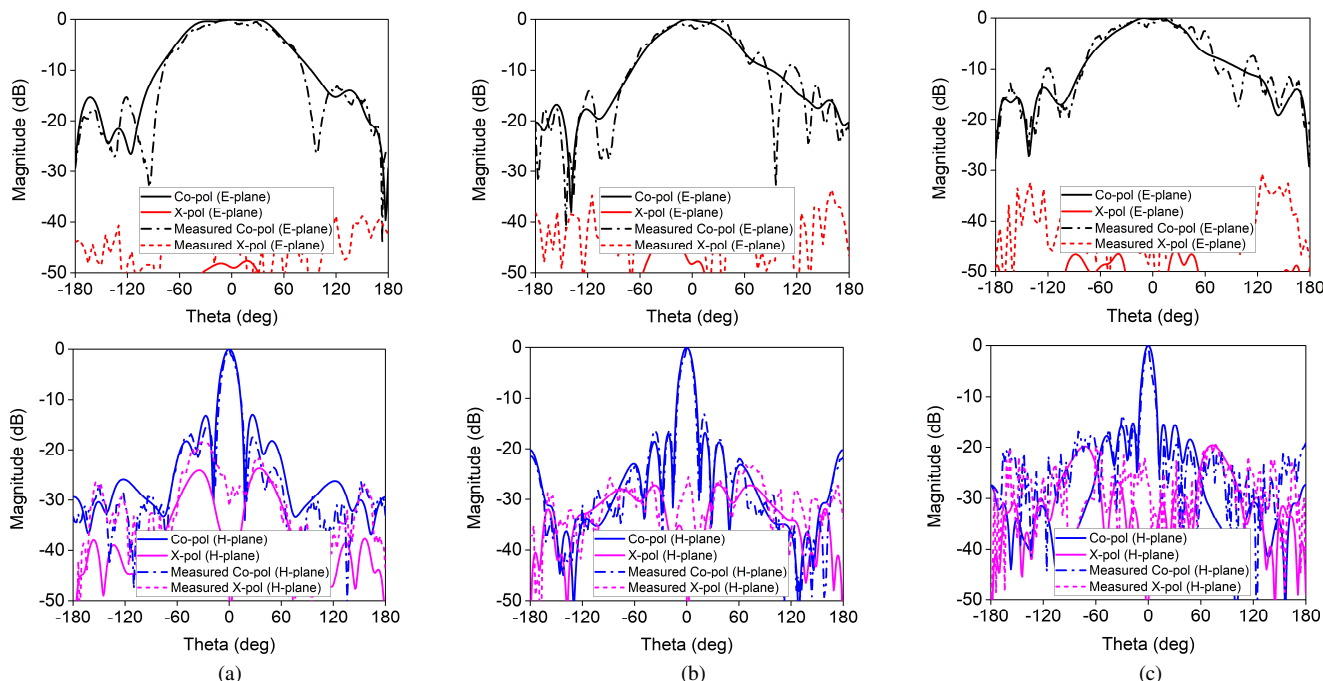

Fig. 16. Measured and simulated normalized radiation pattern of the proposed linear array at (a) 20 GHz, (b) 25 GHz, and (c) 30 GHz.
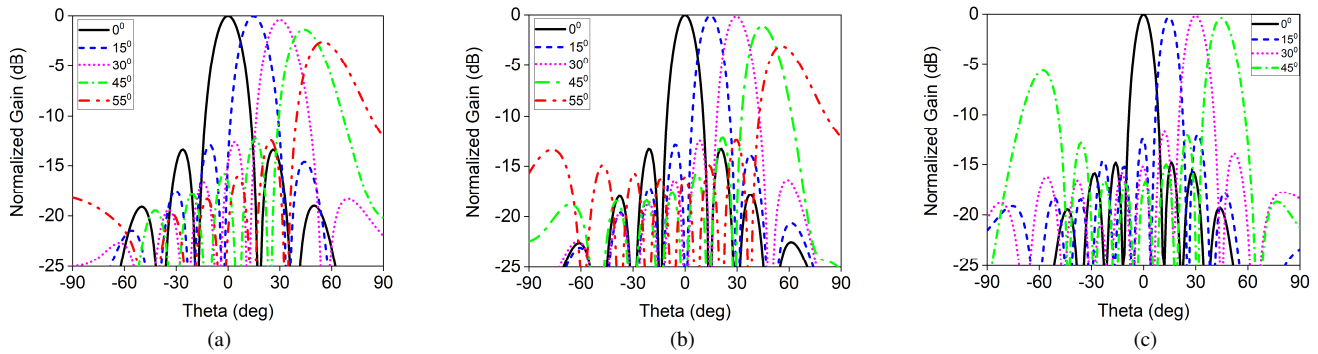
Fig. 17. Simulated beam scanning performance at (a) 20 GHz, (b) 25 GHz, and (c) 31 GHz.

TABLE IV
COMPARISON BETWEEN THE PROPOSED AND REPORTED COMPACT MILLIMETER-WAVE ANTENNA ARRAYS

Reference	Antenna element	Feed network	f_0 (GHz)	Element number	Projected area	Impedance bandwidth	Scanning angles	Efficiency
[21]	Slot	SIW	30	4 x 4	$0.60\,\lambda_0$ x $0.50\,\lambda_0$	13.3%	$\pm69°$	N.A.
[22]	U-slot patch	MSL	27.5	4 x 4	$0.51\,\lambda_0$ x $0.49\,\lambda_0$	22%	$\pm70°$	N.A.
[23]	Tapered slot	SIW	28	1 x 4	$1.10\,\lambda_0$ x $0.50\,\lambda_0$	47%	$\pm35°$ (at f_0)	N.A.
[4]	Transverse slot + ME dipole	SICL	32	1 x 8	$0.64\,\lambda_0$ x $0.45\,\lambda_0$	48.8%	$\pm45°$	71%
[24]	DGS + ME dipole	SICL	35	1 x 16	$0.50\,\lambda_0$ x $0.7\,\lambda_0$	50.7%	$\pm30°$ (at f_0)	70%
This work	RIS + ME dipole	SICL	25	1 x 8	$0.44\,\lambda_0$ x $0.50\,\lambda_0$	48.9%	$\pm45°$	72%

N.A.: not available.

12.2 dB and -5.5 dB, respectively. The increased electrical elementary spacing, in terms of frequency, can explain the significant increase of sidelobe level at 31 GHz. Furthermore, the scan losses at 31 GHz are significantly reduced due to the mutual coupling effect between the array elements deteriorating at higher frequencies. This effect deflects the maximum radiation direction of each element from boresight, compensating for the scan losses at certain angles. For simplicity, the beam scanning performance in the opposite direction is not illustrated, since it can achieve the same performance as pointing at the positive direction due to its symmetric geometry in the *xoz*-plane.

E. Comparison with Other Literature

The existing millimeter-wave compact antenna arrays are listed and compared with the proposed antenna in Table IV. Apart from featuring a smaller projected area, the proposed antenna complements well with the designated SICL feed network to offer a wider overlapped bandwidth than other works in [21]-[23]. Compared with other ME dipole models in [4] and [24], the proposed antenna can still demonstrate competitive performance even though no quarter-wavelength shorted patch is deployed in the element to excite the magnetic dipole mode. Last but not least, the proposed antenna can support $\pm45°$ beam-scanning range for wide frequencies, providing a higher degree of freedom for designing the millimeter-wave applications.

V. CONCLUSION

A novel via-free ME dipole antenna with the SICL feed network has been proposed and investigated. It has been demonstrated that a half-wavelength resonant aperture can replace the conventional quarter-wavelength shorted patch to excite the magnetic dipole mode, significantly reducing the undesired height limitation and fabrication complexity of an ordinary ME dipole antenna. Then, the antenna is further miniaturized by loading the RIS structure, and its radiation properties are shown to be improved. The proposed antenna element supports a wide bandwidth of 64.8% and a high maximum gain of 8.8 dBi. By combining the proposed antenna element with an 8-way parallel SICL feed structure, a linear array with 8 elements is designed, fabricated and analyzed. Competitive and consistent performance are realized across a wide frequency band of 18.7 GHz to 30.8 GHz with SWR ≤ 2. Furthermore, the proposed antenna supports relatively wide beam scanning angles of $\pm45°$ over the wide working frequencies. Hence, the proposed antenna can potentially support the millimeter-wave antenna in package (AiP) and other surface-mounted applications owing to its low profile and promising performance.

REFERENCES

[1] F. Yang and Y. Rahmat-Samii, Electromagnetic Band Gap Structures in Antenna Engineering, Cambridge: Cambridge University Press, 2008.
[2] H. Mosallaei and K. Sarabandi, "Antenna miniaturization and bandwidth enhancement using a reactive impedance substrate," in IEEE Transactions

This article has been accepted for publication in IEEE Transactions on Antennas and Propagation. This is the author's version which has not been fully edited and content may change prior to final publication. Citation information: DOI 10.1109/TAP.2023.3299631

> REPLACE THIS LINE WITH YOUR PAPER IDENTIFICATION NUMBER (DOUBLE-CLICK HERE TO EDIT) <   10

on Antennas and Propagation, vol. 52, no. 9, pp. 2403-2414, Sept. 2004, doi: 10.1109/TAP.2004.834135.

[3] K. M. Luk and H. Wong, "A new wideband unidirectional antenna element," Int. J. Microw. Opt. Technol., vol. 1, no. 1, pp. 35-44, Jun. 2006.

[4] X. Dai, A. Li and K. M. Luk, "A Wideband Compact Magnetoelectric Dipole Antenna Fed by SICL for Millimeter Wave Applications," in IEEE Transactions on Antennas and Propagation, vol. 69, no. 9, pp. 5278-5285, Sept. 2021, doi: 10.1109/TAP.2021.3060146.

[5] L. Ge and K. M. Luk, "A Magneto-Electric Dipole Antenna With Low-Profile and Simple Structure," in IEEE Antennas and Wireless Propagation Letters, vol. 12, pp. 140-142, 2013, doi: 10.1109/LAWP.2013.2244054.

[6] K. Luk and B. Wu, "The Magnetoelectric Dipole—A Wideband Antenna for Base Stations in Mobile Communications," in Proceedings of the IEEE, vol. 100, no. 7, pp. 2297-2307, July 2012, doi: 10.1109/JPROC.2012.2187039.

[7] M. Li, K. M. Luk, Ge L, et al., "Miniaturization of magnetoelectric dipole antenna by using metamaterial loading," IEEE Trans. Antennas Propag., vol. 64, no. 11, pp. 4914-4918, 2016.

[8] N. Engheta and R. Ziolkowski, Metamaterials: Physics and Engineering Explorations, John Wiley & Sons Inc., 2006.

[9] Y. Xu, K. -M. Luk, A. Li and J. Sun, "A Novel Compact Magneto-Electric Dipole Antenna for Millimeter-Wave Beam Steering Applications," in IEEE Transactions on Vehicular Technology, vol. 70, no. 11, pp. 11772-11783, Nov. 2021, doi: 10.1109/TVT.2021.3114217.

[10] L. Cai, H. Wong and K. Tong, "A Simple Low-Profile Coaxially-Fed Magneto-Electric Dipole Antenna Without Slot-Cavity," in IEEE Open Journal of Antennas and Propagation, vol. 1, pp. 233-238, 2020, doi: 10.1109/OJAP.2020.2997816.

[11] L. Cai and K. -F. Tong, "A Millimeter-wave Aperture-coupled Simple Low-Profile Magneto-Electric Antenna," 2020 IEEE Asia-Pacific Microwave Conference (APMC), 2020, pp. 1078-1080, doi: 10.1109/APMC47863.2020.9331721.

[12] M. Li and K. Luk, "Wideband Magneto-Electric Dipole Antenna for 60-GHz Millimeter-Wave Communications," in IEEE Transactions on Antennas and Propagation, vol. 63, no. 7, pp. 3276-3279, July 2015, doi: 10.1109/TAP.2015.2425418.

[13] J. Yin, Q. Wu, C. Yu, H. Wang and W. Hong, "Broadband Symmetrical E-Shaped Patch Antenna With Multimode Resonance for 5G Millimeter-Wave Applications," in IEEE Transactions on Antennas and Propagation, vol. 67, no. 7, pp. 4474-4483, July 2019, doi: 10.1109/TAP.2019.2911266.

[14] J. Xu, W. Hong, Z. H. Jiang, H. Zhang and K. Wu, "Low-Profile Wideband Vertically Folded Slotted Circular Patch Array for Ka-Band Applications," in IEEE Transactions on Antennas and Propagation, vol. 68, no. 9, pp. 6844-6849, Sept. 2020, doi: 10.1109/TAP.2020.3005028.

[15] V. Rathi, G. Kumar and K. P. Ray, "Improved coupling for aperture coupled microstrip antennas," in IEEE Transactions on Antennas and Propagation, vol. 44, no. 8, pp. 1196-1198, Aug. 1996, doi: 10.1109/8.511831.

[16] Aijaz, Z. and S. C. Shrivastava, "Effect of the different shapes: Aperture coupled microstrip slot antenna," International Journal of Electronics Engineering, Vol. 2, No. 1, 103-105, 2010.

[17] Zhu, B., Zhao, J. & Feng, Y, "Active impedance metasurface with full 360° reflection phase tuning," Sci Rep 3, 3059 (2013). https://doi.org/10.1038/srep03059.

[18] Zhang, Z., Chen, W., Fu, J., Li, P., Lv, B. and Wang, Z. (2018), Circularly polarised patch array antenna based on reactive impedance surface. IET Microw. Antennas Propag., 12: 2213-2217. https://doi.org/10.1049/iet-map.2018.5384.

[19] J. Yin, Q. Wu, C. Yu, H. Wang and W. Hong, "Broadband Endfire Magnetoelectric Dipole Antenna Array Using SICL Feeding Network for 5G Millimeter-Wave Applications," in IEEE Transactions on Antennas and Propagation, vol. 67, no. 7, pp. 4895-4900, July 2019, doi: 10.1109/TAP.2019.2916463.

[20] A. Li and K. -M. Luk, "Millimeter-Wave End-Fire Magneto-Electric Dipole Antenna and Arrays With Asymmetrical Substrate Integrated Coaxial Line Feed," in IEEE Open Journal of Antennas and Propagation, vol. 2, pp. 62-71, 2021, doi: 10.1109/OJAP.2020.3044437.

[21] J. -W. Lian, Y. -L. Ban, Q. -L. Yang, B. Fu, Z. -F. Yu and L. -K. Sun, "Planar Millimeter-Wave 2-D Beam-Scanning Multibeam Array Antenna Fed by Compact SIW Beam-Forming Network," in IEEE Transactions on Antennas and Propagation, vol. 66, no. 3, pp. 1299-1310, March 2018, doi: 10.1109/TAP.2018.2797873.

[22] X. Wang, X. Fang, M. Laabs and D. Plettemeier, "Compact 2-D Multibeam Array Antenna Fed by Planar Cascaded Butler Matrix for Millimeter-Wave Communication," in IEEE Antennas and Wireless Propagation Letters, vol. 18, no. 10, pp. 2056-2060, Oct. 2019, doi: 10.1109/LAWP.2019.2937254.

[23] B. Yang, Z. Yu, Y. Dong, J. Zhou and W. Hong, "Compact Tapered Slot Antenna Array for 5G Millimeter-Wave Massive MIMO Systems," in IEEE Transactions on Antennas and Propagation, vol. 65, no. 12, pp. 6721-6727, Dec. 2017, doi: 10.1109/TAP.2017.2700891.

[24] J. Yin, Q. Wu, C. Yu, H. Wang and W. Hong, "Broadband Endfire Magnetoelectric Dipole Antenna Array Using SICL Feeding Network for 5G Millimeter-Wave Applications," in IEEE Transactions on Antennas and Propagation, vol. 67, no. 7, pp. 4895-4900, July 2019, doi: 10.1109/TAP.2019.2916463.

Tsz-Ming Wong was born in Hong Kong, China. He received the B.Eng. degree in electronic and communication engineering from City University of Hong Kong, Hong Kong, in 2019, and the M.Sc. degree in communications and signal processing from Imperial College London, in 2020. He is pursuing the Ph.D. degree in electrical engineering at City University of Hong Kong. His recent research interests focus on millimeter-wave antennas and arrays, transmitarray and reflectarray antennas, and metasurfaces.

Kwai-Man Luk (M'79–SM'94–F'03) is a Fellow of the UK Royal Academy of Engineering and a Fellow of the Hong Kong Academy of Engineering Science. He received the B.Sc.(Eng.) and Ph.D. degrees in electrical engineering from The University of Hong Kong in 1981 and 1985, respectively. He joined the Department of Electronic Engineering at City University of Hong Kong in 1985 as a Lecturer. Two years later, he moved to the Department of Electronic Engineering at The Chinese University of Hong Kong where he spent four years. In 1992, Professor Luk returned to the City University of Hong Kong, where he served as Head of Department of Electronic Engineering from 2004 – 2010 and Director of State Key Laboratory of Millimeter Waves from 2008 – 2013, and is currently Head and Chair Professor of the Electrical Engineering Department. His recent research interests include designs of microstrip patch antennas, magneto-electric dipole antennas, dense dielectric patch antennas and open resonator antennas. He is the author of 4 books, 11 research book chapters, over 400 journal papers and 280 conference papers. He was awarded 16 US and more than 10 PRC patents. He was Technical Program Chairperson of the 1997 Progress in Electromagnetics Research Symposium (PIERS), General Vice-Chairperson of the 1997 and 2008 Asia-Pacific Microwave Conference (APMC), General Chairman of the 2006 IEEE Region Ten Conference (TENCON), Technical Program Co-Chairperson of 2008 International Symposium on Antennas and Propagation (ISAP), and General Co-Chairperson of 2011 IEEE International Workshop on Antenna Technology (IWAT), General Co-Chair of 2014 IEEE International Conference on Antenna Measurements and Applications (CAMA), and General Co-Chair of 2015 International Conference on Infrared, millimeter, and Terahertz Waves (IRMMW-THz 2015). He was the General Chair of the 2020 Asia-Pacific Microwave Conference held in Hong Kong. He is an elected member of the IEEE APS Administrative Committee from 2021 to 2023. He is the Chair of the IEEE APS Distinguished Lecturer Program Committee. He is the Chair of the Fellow Committee of the Electromagnetics Academy.

Professor Luk received the Japan Microwave Prize, at the 1994 Asia Pacific Microwave Conference held in Chiba in December 1994, the Best Paper Award at the 2008 International Symposium on Antennas and Propagation held in Taipei in October 2008 and the Best Paper Award at the 2015 Asia-Pacific Conference on Antennas and Propagation held in Bali in July 2015. He was awarded the very competitive 2000 Croucher Foundation Senior Research Fellow in Hong Kong. He received the 2011 State Technological Invention Award (2nd Honor) of China. He is the recipient of the 2017 IEEE APS John Kraus Antenna Award. He received the prestigious Ho Leung Ho Lee Prize for Science and Technology Progress in 2019 and the 14th Guanghua Engineering Science and Technology Prize in 2022.

He was a Chief Guest Editor for a special issue on "Antennas in Wireless Communications" published in the Proceedings of the IEEE in July 2012, and for a special issue on "Advanced Antennas for Wireless Connectivity" published in Engineering in April 2022. He is a Deputy Editor-in-Chief of PIERS journals and an Associate Editor of IET Microwaves, Antennas and Propagation. Professor Luk is a Fellow of the Chinese Institute of Electronics, PRC, a Fellow of the Institution of Engineering and Technology, UK, a Fellow of the Institute of Electrical and Electronics Engineers, USA and a Fellow of the Electromagnetics Academy, USA.
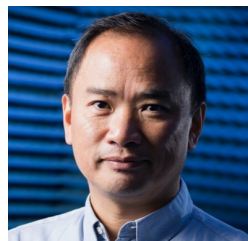
Kin-Fai Tong is a Professor of Antennas and Applied Electromagnetic at UCL. He has a strong track record in novel wideband antennas, circularly polarised patch antenna designs and microwave/mmWave techniques. His career aspiration is to make a real impact to our society through world-leading research activities and innovations, which is evident in his pathway to impact: from fundamental research to innovation, industrial collaboration, patents, commercialisation of technologies, and to engagement with policy makers, schools and the general public. He has published 3 book chapters, 67 peer-reviewed journals and 93 conference papers with an h-index of 28. He is active in knowledge transfer; his Innovate UK project was graded as "OUTSTANDING", i.e., the top 5% among all projects. The project was reported in the Parliamentary Review of UK. He was the winner of the UCL Knowledge Transfer Business of the Year Award 2015, and the 2017 UCL Provost's Spirit of Enterprise Award. He is a Chartered Engineer in the UK, a Fellow of the IEEE, and a Fellow of the Electromagnetics Academy (MIT, USA). He is serving as an Associate Editor of IEEE AWPL, Subject Editor for Antennas for IET Electronics Letters and was the Lead Guest Editor for the IEEE OJAP for the Special Section on Recent Advancements in Liquid Antennas and Their Applications in 2020 and a Guest Editor for the Special Sections on Advanced Antenna Technologies for 5G Internet-of-Things Applications in 2020, and IEEE Journal of Electromagnetics, RF and Microwaves in Medicine and Biology (J-ERM) in 2021. He was the General Chair for the IEEE iWEM 2017, and the TPC Co-Chair of IEEE MTT-S International Microwave Workshop Series on RF and Wireless Technologies for Biomedical and Healthcare Applications. Currently, Prof Tong is also working actively in fluid antennas, surface waves and wideband mmWave transducers for future wireless communications systems.